ACS APPLIED MATERIALS & INTERFACES

Forum Article

www.acsami.org

Pressure-Sensitive Adhesives under the Influence of Relative Humidity: Inner Structure and Failure Mechanisms

Markus Schindler, Manuel Koller, and Peter Müller-Buschbaum*

Physik-Department, Lehrstuhl für Funktionelle Materialien, Technische Universität München, James-Franck-Strasse 1, 85748 Garching, Germany

ABSTRACT: Model pressure-sensitive adhesive (PSA) films of the statistical copolymer P(EHA-*stat*-20MMA), which comprises 80% ethylhexyl acrylate (EHA) and 20% methyl methacrylate (MMA), are studied. The PSA films are stored under different relative humidities from <2% to 96% for 24 h and subsequently investigated concerning the near-surface composition profile by measuring X-ray reflectivity (XRR) and tack performance. For both types of measurements, special custom-made sample environments are used, which ensure constant temperature and relative humidity during the XRR and tack measurements. Different failure mechanisms of the adhesive bond are found by adjusting the relative humidity. XRR measurements evidence enrichment layers in vicinity to and at the surface depending on the provided relative humidity during the postproduction treatment, which also influence the tack performance. This finding is supported by tack measurements using punches with different roughness.

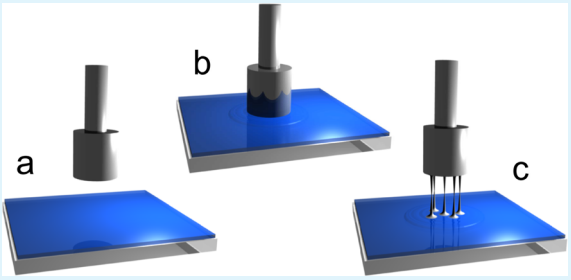

KEYWORDS: *pressure-sensitive adhesive, X-ray reflectivity, tack, failure mechanism, solution casting*

1. INTRODUCTION

Pressure-sensitive adhesives (PSAs) are present in a large variety of applications in science, industries, and every-day life. Showing a wide spectrum of bonding strength, PSAs are applicable not only for low-tack applications, which require an easy and residual-free removal (e.g., protective foils). For the ease of removal it has been shown that the tackiness of a PSA can be switched off via an infrared treatment.[1] Also durable tasks are realized using PSAs, e.g., noise damping in aircrafts.[2] Moreover, PSAs and also other adhesives can join very different kinds of materials such as paper, wood, plastics, and metals,[3−8] and are even applied in medical applications,[9] for instance, to attach patches and sensors to the human skin.[10,11] The origin of this variability of possible applications is found in the chemical nature of the specific polymer and the inner structure of the adhesive film. In the past, a large line-up of tests has been introduced to characterize the adhesive performance of PSAs, among which the rolling ball test,[12] the finger test,[13] the peel test,[14] and the tack-test[3,15,16] are found as well-established and important representatives. Despite their high relevance concerning macroscopic information, they are not capable of giving insights into the inner structure of PSAs in terms of composition gradients or variations of crystallinity and chain conformation. However, this nanoscopic knowledge is of utmost importance for a complete understanding of the origins of the performance of an adhesive in a given situation.

Earlier studies have shown that the near-surface composition can alter the tack performance due to the fact that every adherent penetrates the adhesive to a certain depth, depending on its surface roughness.[17] Diethert et al. showed that the choice of solvent for solution casting of the PSA film and also several postproduction treatments of the PSA film strongly affect the final near-surface composition and thus the tackiness.[18,19] Humidity in the form of adsorbed moisture usually hinders adhesion and plays an important role in aging of adhesive bonds.[20] Moreover, polyacrylates are known to swell in humid environments, also affecting the tack performance.[21] Therefore, the postproduction treatments in this study are based on atmospheres of different relative humidity. Beyond investigations about postproduction treatments of PSA films it is of interest to probe samples under identical conditions as they were used during the sample preparation, because in many realistic bond-and-release applications, the adhesive bond is usually installed and broken under the same conditions. Such a type of investigations need controlled sample environment during preparation and characterization.

X-ray reflectivity (XRR) has proven to be a powerful technique to reveal the inner structure of polymer films in general[22−27] and in particular the near-surface composition of PSAs.[18,19,28] Because of the fact that X-rays interact with the electrons in the atomic shells, it is possible to gather information about the electron density in the vertical direction of the sample on the nanometer scale. The contrast in dispersion between the different components of the PSA film

Special Issue: Forum on Polymeric Nanostructures: Recent Advances toward Applications

Received: September 12, 2014
Accepted: November 14, 2014
Published: November 14, 2014

   dx.doi.org/10.1021/am506265e | *ACS Appl. Mater. Interfaces* 2015, 7, 12319−12327

gives access to the near-surface composition profile. For example, in the case of a model PSA, which comprises two kinds of monomers, ethylhexyl acrylate (EHA) and methyl methacrylate (MMA), XRR can be utilized to identify enrichment layers of one or the other component (dispersion values for the corresponding homopolymers are $\delta_{PEHA} = 4.06 \times 10^{-6}$, $\delta_{PMMA} = 3.21 \times 10^{-6}$,[28]).

In principle, an adhesive bond can exhibit an adhesive or a cohesive failure.[29] Moreover, in the case of PSAs three different failure mechanisms have been observed and also treated theoretically in the past: Cavitation,[30,31] internal,[32,33] and external crack propagation.[34−36] These three failure mechanisms can be grouped in a map of failure mechanisms for the tack test depending on the critical energy dissipation rate, Young's modulus, and punch diameter as a function of the ratio of punch diameter and film thickness (confinement).[29]

In the present study, solution-cast films of a model PSA, a statistical copolymer that consists of 80% ethylhexyl acrylate (EHA) and 20% methyl methacrylate (MMA) denoted P(EHA-*stat*-20MMA), are postproduction treated with different relative humidity and probed with XRR measurements and tack tests under exactly these postproduction conditions. Because of the different polarity of EHA and MMA, a reorganization of the near-surface composition can be observed driven by the polarity of the surrounding atmosphere.[19,28] To be able to provide the same conditions during the measurements as during the treatments, sample environments for the XRR measurements and the tack tests are introduced, which allow for full temperature and atmosphere control. The mechanical behavior obtained by the tack test is correlated with the nanoscopic structure information gathered via XRR. In addition, tack tests with punches of different roughness are performed, because these measurements probe different depths of the adhesive film.

The structure of this article is as follows: After introducing the used materials and sample preparation, the experimental techniques (XRR and mechanical tack test) are explained. Subsequently, the obtained composition profiles and the results for the tack performance are presented and discussed. Finally, the article concludes with a summary of the results and a brief outlook.

2. EXPERIMENTAL SECTION

2.1. Sample Preparation. The statistical copolymer under study is P(EHA-*stat*-20MMA), which consists of 80% ethylhexyl acrylate (EHA) and 20% methyl methacrylate (MMA). EHA represents the soft and sticky majority component with a glass transition temperature of the homopolymer of T_g = 188 K[37] and is responsible for the adhesion of the PSA. A homopolymer of MMA has a glass transition temperature of T_g = 378 K,[37] which is well above room temperature and therefore MMA acts as the glassy component providing sufficient cohesion to the PSA to avoid flow of the adhesive joint. The investigated copolymer had a molecular weight of $M_w = 248 \times 10^3$ g/mol and a rather high polydispersity of $M_w/M_n \approx 4$, which is required for PSAs and resulted from radical solution polymerization in a semibatch procedure in iso-butanol at 100 °C with a peroxide starter (BASF). To remove residual iso-butanol from the synthesis, we evaporated the solvent from the PSA before the sample preparation in a vacuum oven at 150 °C for at least 12 h.

The PSA films were prepared on microscopy glass slides (Carl Roth, 76 × 26 mm^2) via solution casting. The copolymer was dissolved in toluene with a concentration of 94.5 g/L, leading to a thickness of the dry film of approximately 50 ± 5 μm. This value of the film thickness is on the order of adhesive film thickness for real applications, where the adhesive has also to compensate for the roughness of the adherents. The substrates were cleaned before use consecutively with acetone, ethanol and isopropanol and finally dried with compressed oil-free nitrogen. The solution casting was carried out at a constant temperature of 291 ± 1 K in a desiccator with the substrate being perfectly horizontally aligned using a self-aligning laser system. To provide a reproducible relative humidity during the drying of the PSA film, we stored silica gel in the desiccator below the sample, ensuring a relative humidity of below 2%. The limited desiccator volume slowed down the solvent evaporation, which was beneficial to obtain homogeneously flat adhesive films because effects like skinning[38−41] were avoided. The drying lasted for 24 h.

The sample series under investigation comprise adhesive films prepared as explained above, which were postproduction treated with different relative humidities. For this postproduction treatment, the PSAs were stored a second time in desiccators for 24 h, having saturated water-based salt solutions right below the samples. This is a well-established method to install a defined desired relative humidity (RH).[42,43] The used salts were LiCl, $Mg(NO_3)_2 \cdot 6H_2O$, and NaCl. Together with the control sample, which was stored using silica gel (<2% RH), a sample stored under ambient conditions (≈43% RH), and another sample stored using pure water (≈100% RH), a set of six different RHs was realized. With a humidity sensor the real RH values were measured. Due to the opening in the humidity cell for the tack test which is necessary for the punch probe to access the PSA film, the RH in both cells slightly differed. The obtained RH values were <2, 18, 43, 59, 75, and 96% for the XRR cell and 5, 16, 42, 60, 75, and 95% for the tack test cell.

2.2. X-ray Reflectivity. To investigate the composition of the PSA in the near-surface region X-ray reflectivity (XRR) was performed using a Bruker D8 diffractometer. The device was operated with a copper X-ray tube and a focusing Göbel-mirror, resulting in a monochromatic, parallel X-ray beam with a wavelength of 1.54 Å. XRR features a typical vertical resolution on the nanometer to subnanometer scale, which allows for detailed investigations of layered systems. The smallest resolvable length scale depends on the probed q_z range. The maximum depth, which can be investigated by XRR, depends on the specific absorption of the given sample. This so-called scattering depth typically reaches some hundreds of nanometers for polymer films. Due to the thickness of the PSA film of 50 ± 5 μm solely the near-surface region of the adhesive was probed, because absorption of the X-ray beam prevented reflections from interface to the glass substrate. Thus, no information from the bottom interface was superimposed on the gathered XRR data.

The sample was mounted in a custom-designed humidity cell (see section 2.4), which provided full control over temperature and RH. While the body of this cell was made of aluminum, the reservoir for the RH-control substances was made of Teflon to be able to resist among others aggressive salt solutions. Two Kapton windows on front and back allowed the X-rays to pass through the cell. The additional scattering from these Kapton windows was subtracted by fitting a Gaussian function to the high q_z region, in which the Kapton scattering occurred, and subsequently subtracting the fitted curve from the measured XRR data.

For data analysis the fitting software Motofit for IGOR Pro 6.12A with its built-in genetic optimization algorithm was used.[44] To emphasize the features of the reflectivity curves, we chose the so-called Fresnel-normalized representation, where the measured specularly reflected intensity was multiplied by the factor q_z^4 to get rid of the generic decay of the reflectivity. The data were corrected for constant background before this normalization.

2.3. Tack Test. For the mechanical tack-test a custom-designed setup was used, featuring a FGP XF-3030 force sensor and punches made of stainless steel. The punches were cylindrical (radius r = 1 mm) with flat ends, which were polished to different degrees of surface roughness. Atomic force microscopy revealed surface roughness values of 1.7, 6.4, and 105 nm for the three punches used in this study.

To increase the statistical significance of the obtained stress maxima and tack energies, we performed at least 8 repetitions of each tack measurement per sample. Between each measurement the punch was carefully cleaned with a toluene-soaked dust-free tissue and the time

between two subsequent runs was fixed to Δt = 5 min. For each measurement, a fresh spot on the sample was chosen. To be able to follow the failure of the adhesive bond also optically a CCD camera was monitoring the PSA surface from below the sample, whereas the punch approached from the top. The camera was also used to align the punch perfectly parallel with respect to the adhesive film.

For all measurements, the punch approached with a speed of 100 μm/s. As soon as a threshold pressure of 0.32 MPa was detected by the force sensor the movement stopped immediately and the position was kept constant for a dwell time of 10 s. Subsequently, the punch was retracted at a speed of 100 μm/s. During the retraction the measured force and distance were recorded simultaneously. The stress σ was determined by dividing the measured force by the punch area, while the strain ε was obtained by dividing the punch distance from the point of zero stress by the film thickness. The extracted quantities were the maximum stress σ_{max} and the tack energy E_{tack}, which was obtained by integrating the area below the force−distance curve.

A custom-designed cell was implemented to be able to control temperature and RH (see section 2.4). All measurements were carried out at a constant temperature of 291 K.

2.4. Sample Environments. To provide the exact same conditions during the measurements as compared to the post-treatments, we constructed sample environments and implemented in the ray reflectometer and the tack test device. Both custom-made cells have a reservoir to store the substance of choice for installing the desired atmosphere. Figure 1 shows the temporal evolution of the RH

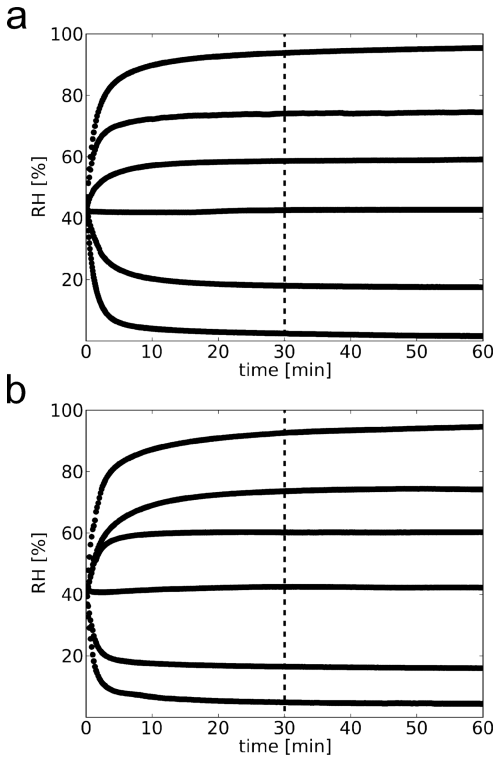

Figure 1. Relative humidity (RH) versus time in the humidity cells for (a) XRR and (b) the tack test. The final RHs for the XRR cell (<2, 18, 43, 59, 75, 96%) differ slightly from those for the tack cell (5, 16, 42, 60, 75, 95%). The dashed vertical lines in both graphs mark the starting point for all measurements.

inside the humidity cell for XRR (Figure 1a) and for the tack test (Figure 1b) after insertion of the desired substances, starting after closing the cells. After 30 min (marked by the vertical dashed lines), only minor changes can be seen, which is why this time was chosen as the starting point of each measurement.

Because of the fact that every X-ray diffractometer in operation heats its interior where the goniometer is located, the sample environment also usually warmed up and deviated from the laboratory temperature. This temperature increase can disturb the precise RH control via the water-based saturated salt solutions. Furthermore, elevated temperatures can also accelerate dynamics in the polymer film. Therefore, it is crucial to provide a temperature control, which was realized by a cooling liquid circulating through the bottom of the humidity cell regulated by a Lauda RC 6 CS.

3. RESULTS AND DISCUSSION

3.1. Composition Profiles. To access the nanoscopic composition of the near-surface region of the PSA under study, XRR measurements are performed using a humidity cell to provide constant temperature and RHs. This kind of experiment is nondestructive, exhibits a resolution on the Ångstroem-scale, has a high statistical relevance due to a large beam footprint and finally a complete composition profile can be extracted out of a single measurement.[45−47] A typical XRR curve is shown in Figure 2 in the Fresnel-normalized representation, which enhances the visibility of weak features on the Fresnel-decay of the intensity.

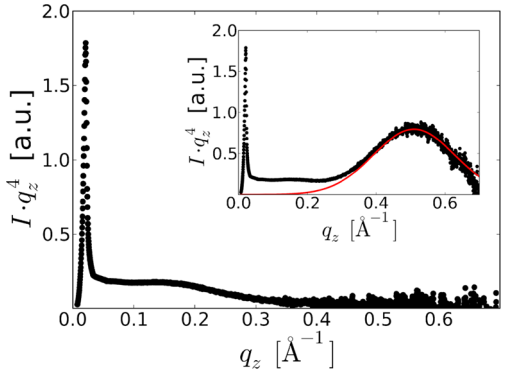

Figure 2. Typical XRR measurement of P(EHA-*stat*-20MMA) film in the Fresnel-normalized representation. The additional scattering from the Kapton windows of the humidity cell (see inset) was fitted with a Gaussian function (red line) and subsequently subtracted to obtain the scattering from the PSA film (main plot).

To reach the sample and the detector, the X-ray beam has to pass the two Kapton windows of the humidity cell, which resulted in additional scattering (see inset of Figure 2). This signal, which is not related to the sample, is fitted with a Gaussian function and subtracted before fitting the reflectivity data. To deduce the near-surface composition of the P(EHA-*stat*-20MMA) films depending on the RH a set of differently post-treated samples is measured and subsequently the reflectivity for each curve is fitted. The results are shown in Figure 3.

All XRR curves exhibit modulations in the low-q_z range, which already indicate nonhomogeneous composition profiles. With increasing RH also the scattering at low q_z values increases, which indicates an enhancement of refractive index contrast in vertical direction. The dispersion profiles, on which the shown fits are based on, are presented in Figure 4a−e. For comparison, a segment length is about 0.6 nm (typical for MMA) and the radius of gyration is about 30 nm if the degree of polymerization is about 2480. However, due to the large polydispersity index, which is common for polymers used as PSAs, the values for the radius of gyration are broadly distributed as well for the used copolymer, which makes a

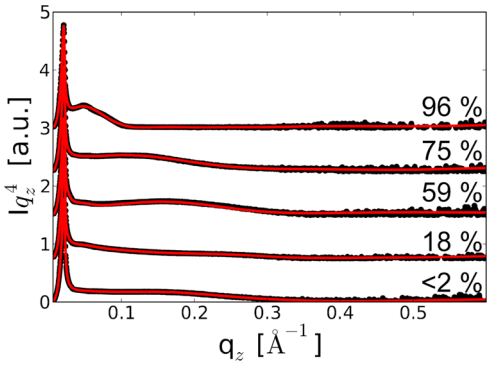

Figure 3. XRR measurements (black dots) and corresponding fits (red lines) for P(EHA-*stat*-20MMA) postproduction treated with different RHs and measured using a temperature controlled humidity cell. The curves are shifted along the *y*-axis for clarity, the RH increases from bottom to top as indicated.

direct comparison of characteristic depths with polymer specific sizes difficult.

Already, the sample post-treated at <2% RH shows an enrichment of the glassy minority component MMA (Figure 4a). This enrichment has already been experimentally observed[19,28,48] and predicted theoretically for similar systems before.[49] Because of the used synthesis in the statistical copolymer, EHA-rich and MMA-rich chains exist and can migrate to the interfaces. Because of the higher solubility of PMMA as compared to PEHA in toluene and the solvent evaporation, MMA-rich polymer chains are preferentially dragged along toward the surface during the solution casting.[49] At an increased RH (18% RH in Figure 4b) more MMA migrates to the film surface and the MMA surface enrichment broadens. For 59% RH (Figure 4c) again a more pure and sharp enrichment layer of the minority component MMA is observed close to the surface followed by two weaker maxima, which get broader with increasing depths. These weaker peaks seem to migrate to smaller depths for 75% RH (Figure 4d). The composition of the sample treated with 96% RH (Figure 4e) shows again a very sharp and clear enrichment layer of MMA, necessarily followed by an EHA enrichment, because both components are covalently bonded in the statistical copolymer. All extracted composition profiles share the weak decay to the mean bulk composition for larger depths from the surface. It has to be noted that the fitting of the XRR data is very sensitive to even subtle changes in the dispersion profiles. Hence, it is possible to reveal also very small compositional modulations in the sample.

Figure 4f shows the depth dependence of the integrated relative MMA content for the investigated different RHs. Obviously, the local MMA content in the near-surface region is higher compared to the bulk content (20%) for all samples. Because of the fact that the XRR fitting is highly sensitive to very subtle changes in the dispersion profile, the integrated relative MMA content has a high significance. It is striking that the MMA content drops only monotonically for the samples treated with <2, 75, and 96% RH, while the other curves show a maximum at a certain depth. The reason for this is found in the driving force for the rearrangement. PMMA has been found to have a polarity of 0.357,[50] whereas the polarity of PEHA is 0.026,[18] which is much smaller. The polarity values represent the ratio of the polar component of the surface tension to the total surface tension. The polarity has been identified to be the driving force behind the changes in the near-surface composition in literature.[19] The sample treated with <2% RH is dry and already close to equilibrium after a total time of 48 h. Also the PSA kept under 96% RH has almost equilibrated due to the strong interaction of the polar environment with the MMA segments in the polymer film. The sample stored at 75% RH exhibits a larger MMA enrichment close to the surface compared to 96% RH. This can be partly explained by residual solvent in the adhesive after the first 24 h. At 75% RH it is easier for the solvent to escape than at 96% RH, because water vapor is known to slow down the solvent evaporation.[19]

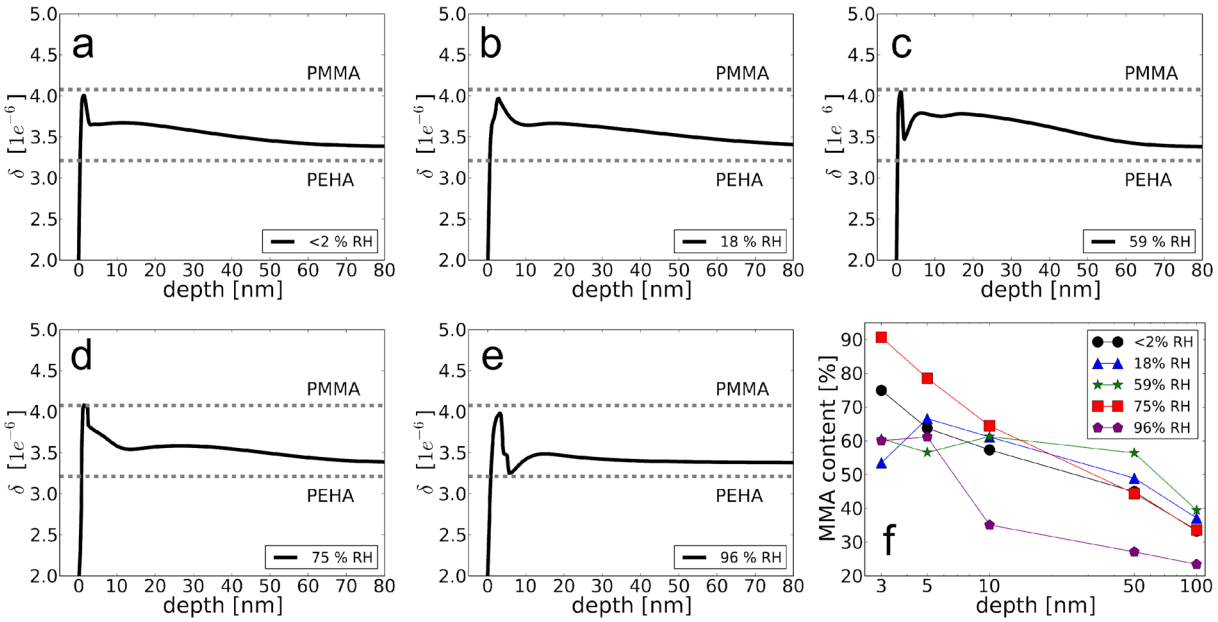

Figure 4. Dispersion profiles of the near-surface region of P(EHA-*stat*-20MMA) films under different RHs: (a) <2% RH, (b) 18% RH, (c) 59% RH, (d) 75% RH, (e) 96% RH. The dashed horizontal lines in each plot mark the dispersion of pure PMMA and pure PEHA, respectively. (f) Integrated MMA content in the near-surface region for different RHs as a function of integration depth.

Therefore, the toluene can still drag MMA chain segments along to the surface. The adhesive films stored under RHs of 18% and 59% show states in-between the lowest and the highest RH. They still reorganize at and near the surface. Hence, when integrating the composition profiles the MMA enrichment at shallow depths appears low, leading to the maxima/plateaus in Figure 4f for 18% and 59% RH. It can also be seen that the MMA enrichment in general decreases with depth, tending asymptotically toward the bulk content of 20%, which is still not reached at a depth of 100 nm.

3.2. Mechanical Behavior with and without Humidity Cell. The postproduction treated adhesive films are investigated using the mechanical tack test as described in the Experimental Section. At first, a series of measurements without and with the use of the humidity cell is compared. Due to our measurement protocol, which comprises at least 8 subsequent measurements being carried out with constant time intervals in-between of Δt = 5 min, it is possible to reveal a time dependency of the stress maximum and the tack energy.

Figure 5 shows a typical stress–strain curve with the stress maximum and the characteristic slow decrease in stress at larger

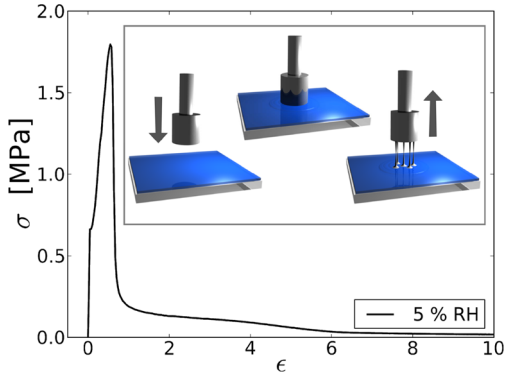

Figure 5. Typical stress–strain curve for a sample postproduction treated at 5% RH. The inset shows schematically the three main steps of the tack measurement: approach of the probe punch, the contact, and finally the retraction.

strain values. The inset depicts the three main steps of a tack measurement: At first, the punch approaches the PSA film and is pressed onto the adhesive with a defined force. After a desired dwell time, the punch is retracted with a controlled speed. From the measured force upon retraction the corresponding stress–strain curve is calculated. The time evolution of the stress maxima σ_{max} for PSA films postproduction treated at three exemplary RHs is compared without (Figure 6) and with the use of the humidity cell (Figure 7) in the tack measurement. The dashed lines in each plot are guides to the eye.

The time series with and without the use of the humidity cell in the tack measurements differ. In case no humidity cell is used (Figure 6), the measured stress maxima show a time dependence in case the RH during the postproduction treatment was different from the ambient RH (42%) during the tack experiment. The values of the stress maxima increase with time for a lower value of the RH during postproduction treatment as compared with the ambient RH (Figure 6a). They decrease with time for a higher RH during postproduction treatment (Figure 6c). The sample post-treated at ambient RH however does not show any major temporal trend (Figure 6b). For the tack energies the same behavior was found. In contrast,

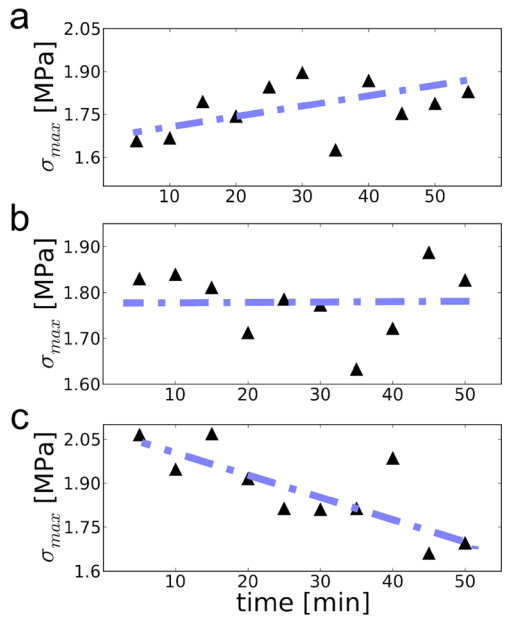

Figure 6. Three exemplary time series of the stress maxima for postproduction treated PSA films at RHs of (a) 5, (b) 42, and (c) 95%, measured without the humidity cell. The dashed lines are guides to the eye.

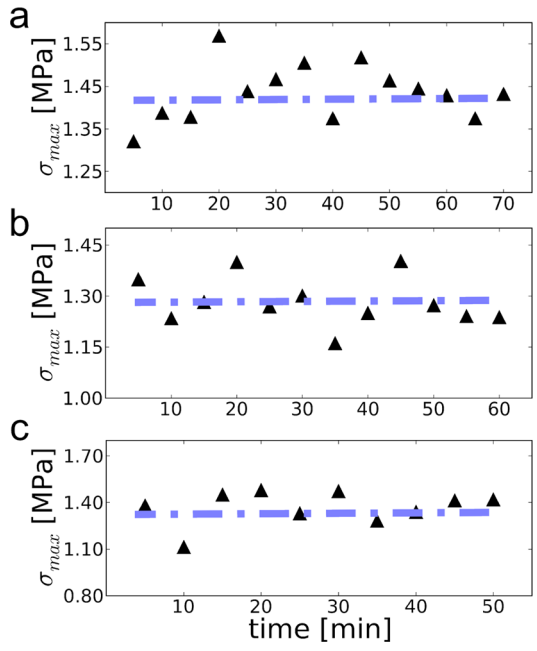

Figure 7. Three exemplary time series of the stress maxima for postproduction treated PSA films at RHs of (a) 5, (b) 42, and (c) 95%, measured with the humidity cell. The dashed lines are guides to the eye.

in case the humidity cell was used during the tack measurement (Figure 7) and thus the measurement was performed at the identical conditions of the postproduction treatment, no trend in the temporal evolution of the stress maxima is seen (Figure 7a-c). This finding already demonstrates the impact of using a humidity cell for the tack measurements. Without humidity cell the PSA films start to change the near-surface composition by adapting to the new RH conditions of the ambient surrounding. In case such temporal evolution would be ignored and the

extracted tack parameters such as stress maxima and tack energies would be averaged, unrealistic large error-bars for the extracted values would result. With the used humidity cell such ongoing modifications of the PSA film can be avoided.

In more detail, the use of the humidity cell introduced additional changes in our measurements. Because the space necessary to implement the humidity cell into the tack device a longer steel punch had to be operated, which had a slightly higher surface roughness (6.4 nm) as compared with the punch used without humidity cell (1.7 nm). This increased punch surface roughness is responsible for the overall lower values of the stress maxima in case the humidity cell was used. However, it is obvious that the measured values exhibit only statistical fluctuations around a temporal constant mean value, which give rise to the typically reported experimental errors.

This proves that the use of a humidity cell is crucial for minimizing error-bars by assuring static conditions also during the measurements. Thus, all further tack measurements are carried out following the procedure explained in the Experimental Section using the custom-designed humidity cell.

3.3. Failure Mechanisms and Tack Performance. After postproduction treatment of the PSA films with different RHs, the mechanical behavior is probed via tack-tests. All tack measurements were carried out at a temperature of 291 K. A constant temperature is crucial for comparable results, because the tackiness of PSAs is sensitive to temperature as well.[51] All recorded stress−strain curves show a rather typical shape of a non-cross-linked PSA: A sharp stress peak at small strains, which is followed by a low stress plateau at higher strains. While for the different RHs below 75% the common cavitation and fibrillation is found, a transition of the failure mechanism is observed at around 75% RH. Figure 8 shows three exemplary stress−strain curves for the three different observed failure mechanisms along with optical micrographs of the adhesive−punch interfaces.

It can be seen that at 75% RH cavitation coexists with internal crack propagation (Figure 8a, b), which leads to very different stress−strain curves. Not only different values of the stress maximum σ_{max} and the tack energy E_{tack} are seen, but also a very abrupt rupture of the adhesive bond is probed in the case of internal crack propagation. Taking the optical micrographs into account, it is clear that at 75% RH both failure mechanisms coexist, even within one detachment (Figure 8b). At high RH such as 95% RH (Figure 8c), only external crack propagation is found. This process is very fast and thus not resolved with the used CCD camera. The adhesive bond ruptures already at significantly lower strains.

Recalling the already mentioned map of failure mechanisms introduced by Creton et al.,[29] it is obvious that the quantities that determine the failure mechanism of a PSA bond are the critical energy release rate G_c and the Young's modulus. Our observation of different failure mechanisms at different RHs shows that the near-surface composition of the PSA plays an important role in combination with the used punch. Using the humidity cell a constant RH is provided also for the steel punch, which is why the surface energy of steel needs to be included in the considerations. Wetting of the punch by water vapor changes the interfacial properties and hence G_c. At the same time dynamic moduli such as the Young's modulus of PMMA is known to decrease with increasing RH.[52] Thus, at different RHs, different dynamical moduli are present, which change the mechanical behavior observable in the tack test. Unfortunately, bulk data of RH dependent dynamic moduli

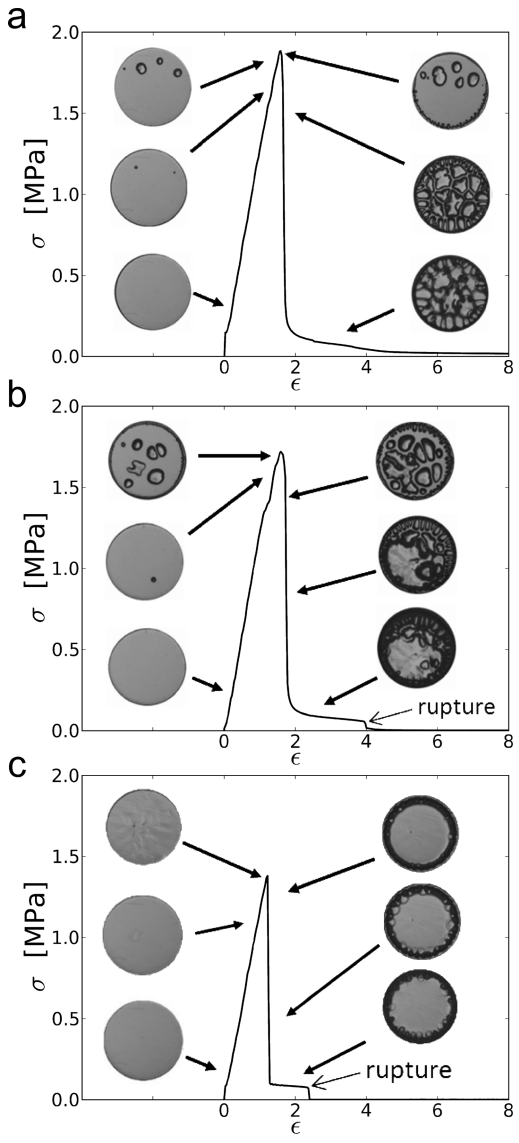

Figure 8. (a) Stress−strain curve for a measurement conducted at 75% RH. The optical micrographs of the adhesive-punch interface show that the bond rupture occurs via cavitation. (b) Stress−strain curve for a measurement also conducted at 75% RH. The micrographs show the coexistence of cavitation and internal crack propagation. (c) Stress−strain curve of a measurement carried out at 95% RH. The micrographs show no cavitation or internal crack propagation. Instead, external crack propagation is found.

cannot be directly used to interpret the findings, because the PSA film has a depth dependent composition, which means that the enrichment layers near the surface will also translate into a depth dependent Young's modulus. Nevertheless, in the present study, we move along the *y*-axis in the map of failure mechanisms, because the confinement (punch diameter divided by the film thickness) is kept constant.

Figure 9 summarizes the measured values of σ_{max} and E_{tack} for the complete set of different RHs, including an identification of the observed failure mechanisms (black dots: cavitation, red triangles: internal crack propagation, blue stars: external crack propagation). A nonmonotonic behavior is found for both parameters.

It can be seen that the value of σ_{max} drops from the first to the second investigated RH to a global minimum and stays

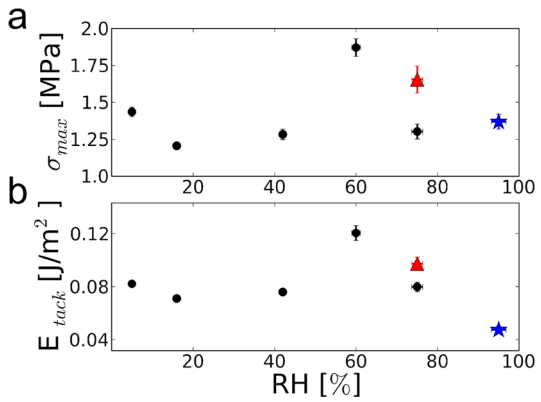

Figure 9. (a) Stress maxima as a function of RH measured with a punch with a surface roughness of 6.4 nm. The black dots mark failure via cavitation and fibrillation, the red triangles represent internal crack propagation and the blue stars denote external crack propagation. (b) Tack energies as a function of RH, using the same color and symbol coding.

rather constant until a sudden increase to the global maximum at 60% RH is observed. For higher RHs the values of the stress maximum drop further, regardless of the failure mechanism. At 75% RH the internal crack propagation shows a higher σ_{max} than obtained in case of cavitation. For 95% RH, σ_{max} stays on a low level. To find an explanation for such complex RH dependence, we compare with the literature.

In earlier experiments Diethert et al. have found MMA enrichment layers in the adhesive near the surface as well.[19] They showed that the amount of MMA near the surface increases monotonically with RH, while also σ_{max} and E_{tack} continuously grow with RH. They attributed this behavior to the enrichment of the glassy MMA near the surface, which disables the PSA to adapt to the roughness of the punch as good as before. As a consequence the effective area of the punch is smaller resulting in a higher pressure, which is in accordance with a theoretical work by Gay et al.[53] In contrast to these earlier studies, we observe a more complex behavior, which can be explained by the use of a humidity cell in the present investigation. Thus, different RHs are present during the tack and XRR measurements as well. As a consequence, the changes in the Young's modulus of the enriched component MMA in the near-surface region need to be taken into account as well. The Young's modulus of PMMA is supposed to get lowered with increasing RH with the steepest drop at around 60% RH.[52] For tack measurements at RHs up to 60% the Young's modulus stays rather constant for PMMA. The XRR measurements have shown a slightly increased roughness at the surface of the PSA films, which lowers the tack performance for these films at RHs from 16% to 75%. At 60% RH, where a global maximum of σ_{max} is present, more MMA has enriched near the surface as compared to lower RHs and its Young's modulus is still on a high level. At higher RH values than 60% σ_{max} drops significantly, because of the softening of Young's modulus.[52]

The determined tack energies follow a similar trend. Nonetheless, at 60% RH the difference in E_{tack} for the two failure mechanisms is not as pronounced, due to the earlier rupture of the bond. This lowers the value of E_{tack} in case of internal crack propagation. For 95% RH the tack energy drops to a global minimum, because of the even earlier complete rupture of the bond.

To understand the complete behavior, competing effects need to be taken into account: An increase in RH is known to enrich MMA near the surface, which in turn improves the tack performance concerning higher values of σ_{max} and E_{tack}. However, an increase in RH also reduces the Young's modulus of PMMA, which reduces these improvements of the tack performance by decreasing of σ_{max} and E_{tack} in a complex way due to the near surface structure of the film. Furthermore, surfaces with high energies (in this case stainless steel) are known to adsorb water vapor,[54] which is also expected to lower the tack performance, because of a reduction of interfacial tension and therefore a reduction of the Dupre work.[55] Because the occurrence of a certain failure mechanism is found to only depend on the RH, but never on time, weakening of the adhesive bond because of water adsorption on the steel surface will have a significant contribution.

3.4. Influence of Punch Roughness. To investigate the influence of punch roughness on this complex behavior, we also used a stainless steel punch with a roughness of 105 nm. The identical experiments as in the case of a small punch roughness are performed. The different failure mechanisms are observed at the same values of the RHs irrespective of the punch roughness. The extracted quantities σ_{max} and E_{tack} from the RH series are shown in Figure 10.

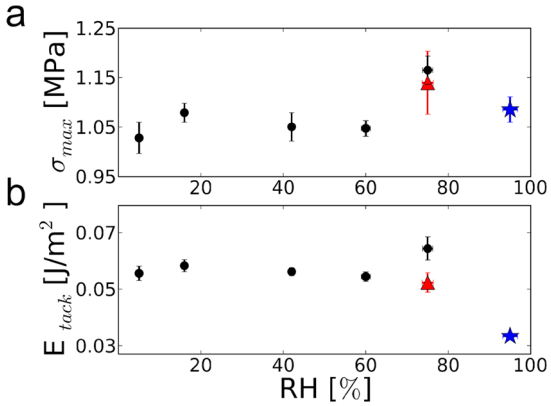

Figure 10. (a) Stress maxima as a function of RH measured with a punch with a surface roughness of 105 nm. The black dots mark failure via cavitation and fibrillation, the red triangles represent internal crack propagation and the blue stars denote external crack propagation. (b) Tack energies as a function of RH, using the same color and symbol coding.

In principle, the same trends are visible as in the case of the low punch roughness, but significantly weaker pronounced, which can be explained by the increased punch roughness. The rougher the punch, the further it penetrates into the adhesive film. The RH postproduction treatment alters the composition of the surfaces and the near-surface region of the PSA strongly in depths up to approximately 20 nm. At larger depths up to about 100 nm still a weak effect of the RH on the composition profile is found. The punch roughness of 105 nm is significantly larger as compared with this heavily influenced region of the PSA film (20 nm), leading to a penetration of the punch into less affected regions of the PSA film. As a consequence, the rougher the punch is, the less sensitive it is concerning changes at and close to the surface. Hence, the features in Figure 8 are damped because the large punch roughness reduced its sensitivity in the tack measurement. In turn, the most sensitive

tack measurements can be performed with very smooth punch surfaces.

4. CONCLUSION

For the first time, the three failure mechanisms cavitation, internal, and external crack propagation are observed in tack tests of P(EHA-*stat*-20MMA) films only by changing the RH. The influence of RH on the tack performance is investigated and correlated with the near-surface composition of the adhesive film on the nanoscale.

XRR has proven to be the technique of choice to obtain fundamental knowledge about the inner composition of the PSA, enabling a correlation of near-surface composition on the nanoscale and macroscopic tack performance. It is shown that the glassy minority component MMA of the statistical copolymer P(EHA-*stat*-20MMA) enriches near the surface as a consequence of the provided polar environment. The main enrichment of MMA is found in a depth of 20 nm below the film surface. Nevertheless, regions of the PSA film deeper than 100 nm (measured from the surface) are affected by the postproduction treatments as well.

Tack tests are performed to link the inner structure of the PSA to its adhesive performance. It is shown that the MMA enrichment can increase the stress maximum. At 60% RH a global maximum of σ_{max} is found. For higher RHs, the Young's modulus of PMMA drops and deteriorates the tack performance. Also the steel punch suffers from adsorption of water at higher RHs leading to weaker bonds. At 75% RH a competition and coexistence of cavitation and internal crack propagation is found. For 95% RH only external crack propagation is observed. Hence, without changing the confinement (ratio of punch diameter and film thickness) all three failure mechanisms are evidenced. The use of a probe punch with a roughness of 105 nm, which is similar to the maximum depth of the shown composition profiles, shows similar but weaker trends, if compared to the flat punch with a roughness of 6.4 nm. This again underlines that the effect of MMA enrichment is strongest very close at the surface and is in very good agreement with the results obtained from XRR.

In more general, different RH strongly influence the tack performance of PSA films if a mobility of the PSA components allows for a reorientation of the molecular near-surface composition. Such effects are the more pronounced, the less rough adherent surfaces are bonded. For extremely flat adherent surfaces in turn a change in RH allows to switch the adhesive behavior. Thus, in such scenario RH can be used as an external trigger for, for example, weakening PSA bonding, and thereby facilitate the debonding of a PSA joint.

AUTHOR INFORMATION

Corresponding Author

*E-mail: muellerb@ph.tum.de. Phone: +49 89 289 12451. Fax: +49 89 289 12 473.

Notes

The authors declare no competing financial interest.

ACKNOWLEDGMENTS

This work has been supported by the GreenTech Initiative—Interface Science for Photovoltaics (ISPV) of the EuroTech Universities together with the International Graduate School of Science and Engineering (IGSSE), TUM.

REFERENCES

(1) Gurney, R. S.; Dupin, D.; Nunes, J. S.; Ouzineb, K.; Siband, E.; Asua, J. M.; Armes, S. P.; Keddie, J. L. Switching off the Tackiness of a Nanocomposite Adhesive in 30 s via Infrared Sintering. *ACS Appl. Mater. Interfaces* **2012**, *4*, 5442−5452.

(2) Rao, M. D. Recent Applications of Viscoelastic Damping for Noise Control in Automobiles and Commercial Airplanes. *J. Sound Vib.* **2003**, *262*, 457−474.

(3) Müller-Buschbaum, P.; Ittner, T.; Maurer, E.; Körstgens, V.; Petry, W. Pressure-Sensitive Adhesive Blend Films for Low-Tack Applications. *Macromol. Mater. Eng.* **2007**, *292*, 825−834.

(4) Severtson, S. J.; Wang, X.; Kroll, M. S. Development of Environmentally Benign Pressure-Sensitive Adhesive Systems via Modification of Substrate Properties. *Ind. Eng. Chem. Res.* **2002**, *41*, 5668−5675.

(5) Maurer, E.; Loi, S.; Wulff, D.; Willenbacher, N.; Müller-Buschbaum, P. Microscopic Structure in Pressure Sensitive Adhesives: an Ultra Small Angle X-ray Study. *Phys. B (Amsterdam, Neth.)* **2005**, *357*, 144−147.

(6) Steven-Fountain, A. J.; Atkins, A. G.; Jeronimidis, G.; Vincent, J. F.; Farrar, D. F.; Chivers, R. A. The Effect of Flexible Substrates on Pressure-Sensitive Adhesive Performance. *Int. J. Adhes. Adhes.* **2002**, *22*, 423−430.

(7) Krüger, J.-K.; Possart, W.; Bactavachalou, R.; Müller, U.; Britz, T.; Sanctuary, R.; Alnot, P. Gradient of the Mechanical Modulus in Glass-Epoxy-Metal Joints as measured by Brillouin Microscopy. *J. Adhes.* **2004**, *80*, 585−599.

(8) Bockenheimer, C.; Valeske, B.; Possart, W. Network Structure in Epoxy Aluminium Bonds after Mechanical Treatment. *Int. J. Adhes. Adhes.* **2002**, *22*, 349−356.

(9) Yang, S. Y.; O'Cearbhaill, E. D.; Sisk, G. C.; Park, K. M.; Cho, W. K.; Villiger, M.; Bouma, B. E.; Pomahac, B.; Karp, J. M. A Bio-Inspired Swellable Microneedle Adhesive for Mechanical Interlocking with Tissue. *Nat. Commun.* **2013**, *4*, 1702.

(10) Minghetti, P.; Cilurzo, F.; Tosi, L.; Casiraghi, A.; Montanari, L. Design of a new Water-Soluble Pressure-Sensitive Adhesive for Patch Preparation. *AAPS PharmSciTechnol.* **2003**, *4*, 53−61.

(11) Woolfson, A. D. Moisture-Activated, Electrically Conducting Bioadhesive Interfaces for Biomedical Sensor Applications. *Analyst* **1996**, *121*, 711−714.

(12) González, I.; Leiza, J. R.; Asua, J. M. Exploring the Limits of Branching and Gel Content in the Emulsion Polymerization of n-BA. *Macromolecules* **2006**, *39*, 5015−5020.

(13) Kamagata, K.; Saito, T.; Toyama, M. The Methods of Measuring Tackiness of Pressure Sensitive Adhesive Tapes. *J. Adhes.* **1970**, *2*, 279−291.

(14) Amouroux, N.; Petit, J.; Léger, L. Role of Interfacial Resistance to Shear Stress on Adhesive Peel Strength. *Langmuir.* **2001**, *17*, 6510−6517.

(15) Agirre, A.; Nase, J.; Degrandi, E.; Creton, C.; Asua, J. M. Improving Adhesion of Acrylic Waterborne PSAs to Low Surface Energy Materials: Introduction of Stearyl acrylate. *J. Polym. Sci., Part A: Polym. Chem.* **2010**, *48*, 5030−5039.

(16) Zosel, A. The Effect of Fibrilation on the Tack of Pressure Sensitive Adhesives. *Int. J. Adhes. Adhes.* **1998**, *18*, 265−271.

(17) Peykova, Y.; Guriyanova, S.; Lebedeva, O. V.; Diethert, A.; Müller-Buschbaum, P.; Willenbacher, N. The Effect of Surface Roughness on Adhesive Properties of Acrylate Copolymers. *Int. J. Adhes. Adhes.* **2010**, *30*, 245−254.

(18) Diethert, A.; Müller-Buschbaum, P. Probing the Near-Surface Composition Profile of Pressure Sensitive Adhesive Films with X-Ray Reflectivity. *J. Adhes.* **2011**, *87*, 1167−1190.

(19) Diethert, A.; Ecker, K.; Peykova, Y.; Willenbacher, N.; Müller-Buschbaum, P. Tailoring the Near-Surface Composition Profiles of Pressure-Sensitive Adhesive Films and the Resulting Mechanical Properties. *ACS Appl. Mater. Interfaces.* **2011**, *3*, 2012−2021.

(20) Meiser, A.; Willstrand, K.; Possart, W. Influence of Composition, Humidity, and Temperature on Chemical Aging in

Epoxies: A Local Study of the Interphase with Air. *J. Adhes.* **2010**, *86*, 222−243.
(21) Chen, W.-L.; Shull, K. R.; Papatheodorou, T.; Styrkas, D. A.; Keddie, J. L. Equilibrium Swelling of Hydrophilic Polyacrylates in Humid Environments. *Macromolecules.* **1999**, *32*, 136−144.
(22) Russell, T. P. X-ray and Neutron Reflectivity for the Investigation of Polymers. *Mater. Sci. Rep.* **1990**, *5*, 171−271.
(23) Lvov, Y.; Decher, G.; Haas, H.; Möhwald, H.; Kalachev, A. X-ray Analysis of Ultrathin Polymer Films Self-Assembled onto Substrates. *Phys. B (Amsterdam, Neth.)* **1994**, *198*, 89−91.
(24) Yu, W.; Yang, D.; Zhu, X.; Wang, X.; Tu, G.; Fan, D.; Zhang, J.; Li, C. Control of Nanomorphology in All-Polymer Solar Cells via Assembling Nanoaggregation in a Mixed Solution. *ACS Appl. Mater. Interfaces.* **2014**, *6*, 2350−2355.
(25) Fladischer, S.; Neuhold, A.; Kraker, E.; Haber, T.; Lamprecht, B.; Salzmann, I.; Resel, R.; Grogger, W. Diffusion of Ag into Organic Semiconducting Materials: A Combined Analytical Study Using Transmission Electron Microscopy and X-ray Reflectivity. *ACS Appl. Mater. Interfaces.* **2012**, *4*, 5608−5612.
(26) Foster, M.; Stamm, M.; Reiter, G. X-ray Reflectometer for Study of Polymer Thin Films and Interfaces. *Vacuum.* **1990**, *41*, 1441−1444.
(27) Liu, Y.; Reiter, G.; Kunz, K.; Stamm, M. Investigation of the Interdiffusion between Poly (methyl methacrylate) Films by Marker Movement. *Macromolecules.* **1993**, *26*, 2134−2136.
(28) Schindler, M.; Kriele, A.; Müller-Buschbaum, P. Reorganization of the Near-Surface Composition in Pressure Sensitive Adhesive Films Stored in Nitrogen Atmosphere. *J. Adhes.* **2012**, *88*, 684−698.
(29) Creton, C.; Fabre, P. In *Adhesion Science and Engineering*; Dillard, D. A., Chaudhury, M., Pocius, A. V., Eds.; Elsevier: Amsterdam, 2002; Chapter 1, pp 535−576.
(30) Green, A. E.; Zerna, W. *Theoretical Elasticity*; Clarendon Press: Oxford, U.K., 1954.
(31) Gent, A. N.; Lindley, P. B. Tension Flaws in Bonded Cylinders of Soft Rubber. *Rubber Chem. Technol.* **1958**, *31*, 393−394.
(32) Sneddon, I. The Distribution of Stress in the Neighbourhood of a Crack in an Elastic Solid. *Proc. R. Soc. London, Ser. A* **1946**, *187*, 229−260.
(33) Crosby, A. J.; Shull, K. R.; Lakrout, H.; Creton, C. Deformation and Failure Modes of Adhesively Bonded Elastic Layers. *J. Appl. Phys.* **2000**, *88*, 2956−2966.
(34) Ganghoffer, J. F.; Gent, A. N. Adhesion of a Rigid Punch to a Thin Elastic Layer. *J. Adhes.* **1995**, *48*, 75−84.
(35) Ganghoffer, J. F.; Schultz, J. An Analytical Model of the Mechanical Behaviour of Elastic Adhesively Bonded Joints. *J. Adhes.* **1996**, *55*, 285−302.
(36) Shull, K. R.; Ahn, D.; Chen, W.-L.; Flanigan, C. M.; Crosby, A. J. Axisymmetric Adhesion Tests of Soft Materials. *Macromol. Chem. Phys.* **1998**, *199*, 489−511.
(37) Cannon, L. A.; Pethrick, R. A. Effect of the Glass-Transition Temperature on Film Formation in 2-Ethylhexyl Acrylate/Methyl Methacrylate Emulsion Copolymers. *Macromolecules* **1999**, *32*, 7617−7629.
(38) Cairncross, R. A.; Durning, C. J. A Model for Drying of Viscoelastic Polymer Coatings. *AIChE J.* **1996**, *42*, 2415−2425.
(39) Edwards, D. A. Trapping Skinning in Polymers: Theoretical Predictions. *Chem. Eng. Commun.* **1998**, *166*, 201−216.
(40) Cairncross, R. A.; Francis, L. F. Le Scriven Predicting Drying in Coatings that React and Gel: Drying Regime Maps. *AIChE J.* **1996**, *42*, 55−67.
(41) Tsige, M.; Grest, G. S. Solvent Evaporation and Interdiffusion in Polymer Films. *J. Phys.: Condens. Matter* **2005**, *17*, 4119.
(42) Giahi, A.; El Alaoui Faris, M.; Bassereau, P.; Salditt, T. Active Membranes Studied by X-ray Scattering. *Eur. Phys. J. E* **2007**, *23*, 31−437.
(43) Leonard, M. J.; Strey, H. H. Phase Diagrams of Stoichiometric Polyelectrolyte-Surfactant Complexes. *Macromolecules* **2003**, *36*, 9549−9558.
(44) Nelson, A. Co-Refinement of Multiple-Contrast Neutron/X-ray Reflectivity Data using MOTOFIT. *J. Appl. Crystallogr.* **2006**, *39*, 273−276.
(45) Diethert, A.; Peykova, Y.; Willenbacher, N.; Müller-Buschbaum, P. Near-Surface Composition Profiles and the Adhesive Properties of Statistical Copolymer Films being Model Systems of Pressure Sensitive Adhesive Films. *ACS Appl. Mater. Interfaces* **2010**, *2*, 2060−2068.
(46) Born, M., Wolf, E. *Principles of Optics*; Pergamon Press: London, 1959.
(47) James, R. W. *The Optical Principles of the Diffraction of X-Rays*; G. Bell and Sons: London, 1962.
(48) Schindler, M.; Pröller, S.; Geue, T.; Müller-Buschbaum, P. Near-Interface Composition in Pressure Sensitive Adhesives at the Adhesive-Adherent Interface. *Macromol. React. Eng.* **2013**, *7*, 549−554.
(49) Donley, J. P.; Fredrickson, G. H. Properties of Random Multiblock Copolymer Melts near Surfaces. *Macromolecules.* **1994**, *27*, 458−467.
(50) PigŁowski, J. M.; Bryjak, M. Surface Studies of Poly (methyl methacrylate)/Poly (styrene-co-acrylonitrile) Blends. *Eur. Polym. J.* **1998**, *34*, 1669−1673.
(51) O'Connor, A. E.; Willenbacher, N. The Effect of Molecular Weight and Temperature on Tack Properties of Model Polyisobutylenes. *Int. J. Adhes. Adhes.* **2004**, *24*, 335−346.
(52) Nolte, A. J.; Treat, N. D.; Cohen, R. E.; Rubner, M. F. Effect of Relative Humidity on the Young's Modulus of Polyelectrolyte Multilayer Films and Related Nonionic Polymers. *Macromolecules.* **2008**, *41*, 5793−5798.
(53) Gay, C.; Leibler, L. Theory of Tackiness. *Phys. Rev. Lett.* **1999**, *82*, 936−939.
(54) Kinloch, A. J. *Adhesion and Adhesives: Science and Technology*; Springer: Heidelberg, 1987.
(55) Israelachvili, J. N. *Intermolecular and Surface Forces*, 3rd ed; Elsevier: Waltham, MA, 2011.